Intermolecular structure in tri-n-butyl phosphate/n-octane mixtures: a molecular dynamics simulation study

Author(s): Anirban Mondal and Sundaram Balasubramanian

Source: *Current Science*, Vol. 106, No. 9 (10 May 2014), pp. 1235-1242
Published by: Current Science Association
Stable URL: https://www.jstor.org/stable/24102339
Accessed: 28-04-2021 18:43 UTC

Intermolecular structure in tri-*n*-butyl phosphate/*n*-octane mixtures: a molecular dynamics simulation study

Anirban Mondal and Sundaram Balasubramanian*

Chemistry and Physics of Materials Unit, Jawaharlal Nehru Centre for Advanced Scientific Research, Bangalore 560 064, India

Tri-*n*-butyl phosphate (TBP) is an important extractant for heavy metal ions. The microscopic structure of TBP/*n*-octane mixtures as a function of concentration of TBP is examined through atomistic molecular dynamics simulations. A weak association between TBP molecules both in pure TBP as well as in the octane solution is established. In dilute TBP/*n*-octane solutions, TBP molecules are inhomogeneously distributed. Structural results from simulations are compared with experimental X-ray and neutron scattering data. Features are assigned through calculations of partial structure factors.

Keywords: Atomistic molecular dynamics, heavy metal extraction, *n*-octane, structure factor, tri-*n*-butyl phosphate.

Introduction

IN the field of solvent extraction, liquid–liquid extraction is the most common technique to separate compounds. In this method, compounds are separated based on their relative solubilities in two immiscible liquids; most often the two liquids happen to be water and an organic solvent. This technique, used to extract a substance from one liquid phase to another, finds wide applications in heavy metal extraction and reprocessing of nuclear waste. In the latter, the separation and recovery of plutonium, uranium, zirconium, etc. from irradiated nuclear fuel is crucial[1–3]. In the solvent extraction methods for nuclear fuel recycling, often the organic phase consists of a mixture of an extracting agent and a diluent.

An important family of extractant molecules are the neutral organophosphorus ligands[4], which bind the cations via their phosphoryl group. Among them, the most widely employed species is tri-*n*-butyl phosphate (TBP)[5]. It has been used to extract uranium[6], plutonium[7], zirconium[8] and other metal ions[9]. Liquid TBP is miscible in organic solvents such as chloroform while barely so in water, which property can be exploited in heavy metal extraction. In the liquid–liquid extraction process, the organic components get separated into two phases, a light one and a heavy organic phase. The latter is known as the third phase and consists of a high concentration of metals and TBP[10–12].

At room temperature, TBP is a liquid (boiling point = 284° ± 5°C, freezing point ≈ –80°C, and density at 25°C = 0.9727 g cm^{-3})[13]. All neutral organophosphorus compounds exhibit a tendency to self-associate and TBP also follows this general trend[14–18]. Its self-association has been brought out with a variety of techniques, including distribution experiments[19], infrared spectroscopy[20], nuclear magnetic resonance[14], calorimetry[16,17], and vapour pressure osmometry[18]. These techniques have also been used to explain the interaction between TBP and various solvents such as CCl_4, $CHCl_3$ and benzene. In hexane, the positive nonideality accounts for the self-association of TBP. On the contrary, in other diluents the negative nonideality refers to TBP–diluent interaction, i.e. interaction between the phosphoryl oxygen and the π-electrons of benzene, hydrogen bonding between phosphoryl oxygen and chloroform, and the interaction of the vacant 3*d*-orbital of chlorine and the phosphoryl oxygen. The existence of hydrogen bonding between TBP and chloroform has also been ascertained through proton magnetic resonance studies[21].

These investigations have revealed that dipole–dipole interactions between P=O groups of the phosphate ester are responsible for the self-association of TBP[13,14,19,20,22]. Alcock *et al.*[23] have studied the TBP–water system to explain the hydrogen bonding between phosphoryl oxygen and water proton, which leads to the formation of a monohydrate compound such as TBP·H_2O that exists in organic phase. Osseo-Asare[24] examined the TBP–diluent/H_2O–acid–metal ion extraction systems. He proposed the existence of a highly ordered assembly (such as a micelle or micro emulsion) of TBP–acid–metal ion complex in organic diluents. The self-assembled framework consists of a hydrophilic core and a hydrophobic shell. The former is polar in nature and is composed of P=O groups of TBP and hence is capable of incorporating heavy metal ions. On the other hand, the hydrophobic shell is composed of the larger butyl tails of TBP, which is swollen by the diluent. In later years, progress was made to understand the formation, mechanism and structure (size, shape and aggregation number) of high-order assemblies in the

*For correspondence. (e-mail: bala@jncasr.ac.in)

organic phase by small-angle X-ray and neutron scattering (SAXS and SANS) techniques. Erlinger *et al.*[25] studied the microscopic structures of reverse micelles of malonamides in organic phases using the Baxter sticky hard sphere model[26–28]. They suggested that the van der Waals interactions between the malonamide reverse micelles in organic phase are the origin for the formation of the third phase. Since then, Chiarizia *et al.*[29] have studied the small-angle scattering profiles for organic phases containing TBP and heavy metal ions using the same hard sphere model. Recently, Motokawa *et al.*[30] have studied the TBP/*n*-octane systems in dry conditions (without water) to reveal the microscopic structure of TBP assemblies in a dry diluent through analysis of the SAXS and SANS profiles. They suggested a weak attraction between TBP molecules in *n*-octane to result in ellipsoidal TBP assemblies.

In recent years, molecular modelling studies have been employed to understand the fundamental molecular level behaviour of extraction systems. Molecular dynamics studies have been carried out by Wipff and co-workers to study systems such as TBP in vacuum and in chloroform[31], the stoichiometry of TBP complexation in aqueous solution[32], TBP complexation with uranyl nitrate and dissolution in supercritical CO_2 (ref. 33), the effect of TBP concentration and water acidity at the water–oil interface[34], and liquid–liquid extraction of pertechnetic acid by TBP[35]. Almeida and co-workers have performed a series of molecular dynamics simulations to illustrate the aqueous phase complex formation process, interfacial migration and the effect of interface in promoting the formation of various complex species, and the migration of neutral species into the organic phase[36–38].

To our knowledge, no simulations have been carried out for TBP in a dry diluent. In this work, we present a classical molecular dynamics simulation study of TBP in *n*-octane to provide an important glimpse into the initial state of the organic phase prior to the extraction of heavy metal ions. Anticipating our results, we find the weak aggregation of TBP molecules leading to the formation of a dimer in which the P=O vectors of neighbouring molecules are either antiparallel or perpendicular to each other. The calculated scattering profiles as a function of concentration of diluent compare well with the experimental data of Motokawa *et al.*[30].

Computational details

A schematic of the TBP molecule is shown in Figure 1. Classical molecular dynamics simulations were performed on TBP/*n*-octane solutions over the entire range of mole fractions. Densities of pure systems calculated from these simulations agree well with experiments[39,40]. Initial simulations were carried out on small system sizes (containing a maximum of 400 TBP molecules and 1500 *n*-octane molecules) to try and understand the solution and to identify the length scale of emerging intermolecular correlations. Larger system sizes were required as TBP molecules were seen to aggregate in *n*-octane. Results from these larger simulations are reported here. Volume fractions studied along with the number of molecules employed are shown in Table 1.

An all-atom model based on the OPLS (optimized potentials for liquid simulations) force field developed by Cui *et al.*[41] was used for TBP, whereas for *n*-octane the TraPPE united atom model was used[42]. Initial configurations were generated using the Packmol software package[43]. Equations of motion were integrated with the velocity Verlet algorithm with a time step of 0.5 fs. A cut-off of 15 Å was chosen for calculating pairwise interactions in real space. Long-range electrostatic interactions were computed using the particle–particle particle–mesh solver with a precision of 10^{-5}. The non-bonded interactions calculated for a pair of atoms in TBP separated by three bonds (1–4 interaction) were applied with scaling factors 1/2 and 1/1.2 for van der Waals and electrostatics respectively. The parameters for cross interactions between different molecular species (atomic groups) were derived using the standard Lorentz–Berthelot rules. Three-dimensional cubic periodic boundary conditions were applied. Tail corrections to the energy and pressure were applied.

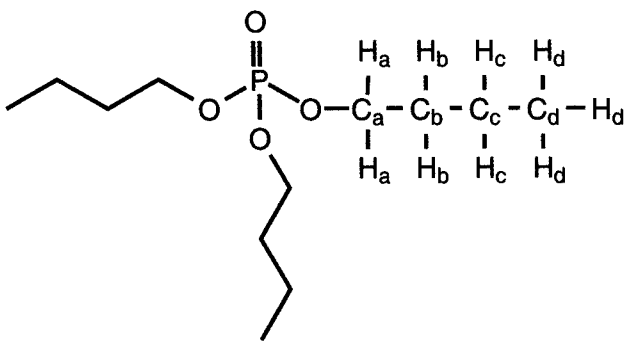

Figure 1. Schematic of tri-*n*-butyl phosphate (TBP). The oxygen atom double bonded to phosphorus is of type O2, while the single-bonded one is of type OS. Carbon and hydrogen atoms on two alkyl tails are not shown for clarity.

Table 1. Summary of different systems studied

Volume fraction of tri-*n*-butyl phosphate (TBP; %)	No. of TBP molecules	No. of *n*-octane molecules
100	2000	0
90	1800	334
75	1500	835
50	1000	1670
25	500	2505
10	200	3006
0	0	500

Classical molecular dynamics simulations at constant number of molecules and constant temperature of 298 K were performed. Temperature and pressure of the systems were maintained at 298 K and 1 atm using the Nóse–Hoover thermostat and barostat respectively, with a damping factor of 1 ps. Initial configurations were relaxed using standard energy minimization methods. Constant pressure and constant temperature ensemble (NPT) simulations were carried out on these energy-minimized configurations until the volume equilibrated. The final coordinates of the NPT run were used as initial configuration for the constant-volume and constant-temperature (NVT) ensemble runs for further equilibration over 8 ns. Finally, for each concentration, an analysis run was generated for 5 ns in which configurations were stored every 0.25 ps. Simulations were carried out using the LAMMPS software package[44]. All systems were visualized using VMD[45].

Partial pair correlation functions were obtained with a bin width of 0.02 Å for all distinct pairs of atom types, up to a distance of half the box length. These partial pair correlation functions were then used to obtain the isotropic partial structure factors.

The isotropically averaged partial structure factor between a pair of atom types α and β is given by[46]

$$S_{\alpha\beta}(q) = \delta_{\alpha\beta} + 4\pi\sqrt{\rho_\alpha \rho_\beta}\int_0^\infty r^2[g_{\alpha\beta}(r)-1]\frac{\mathrm{Sin}(qr)}{qr}\mathrm{d}r, \quad (1)$$

where $\rho_\alpha = N_\alpha/V$. N_α is the number of atoms of type α and V the volume of the system, δ the Kronecker delta function and $g(r)$ is the pair correlation function. The upper limit in the integral was replaced with half the box length. The total X-ray structure factor is defined as

$$S(q) = \sum_\alpha \sum_\beta c_{\alpha\beta}\frac{f_\alpha(q) f_\beta(q)}{\langle f(q)\rangle^2} S_{\alpha\beta}(q), \quad (2)$$

where c_α is the concentration of atom type α in the system. f_α is the form factor of the atom type α and $\langle f(q)\rangle = \sum_\alpha c_\alpha f_\alpha(q)$.

The minimum value of q in our calculation was set by the linear dimension of the simulation box. The box length for all of our large systems was in the neighbourhood of 96 Å. Therefore, the lowest value of q was around 0.065 Å^{-1}. The X-ray form factors for all atom types were obtained from the NIST X-Ray Form Factors, Attenuation and Scattering Tables[47,48]. The values of form factors for each atom type are needed at integral multiples of the smallest q, which depends on the length of the simulation box. The values of form factors obtained from the tables[47,48] were linearly interpolated to obtain form factors at the desired q values.

The total neutron structure factor was also obtained from the partial pair correlation functions. Here, the q-independent neutron scattering length of all the different atom types replaces the atom form factors described above. These scattering lengths were obtained from NIST Neutron scattering lengths and cross-sections Table[47,48]. Hydrogen possesses a large incoherent scattering cross-section; thus, scattering experiments have been carried out in perdeuterated octane[30]. In order to compare against these experiments, we too have considered perdeuterated *n*-octane molecules in our calculations for the scattering profiles, while maintaining hydrogens in case of alkyl tails in TBP.

The total X-ray and neutron scattering intensities were calculated as the square of total structure factors for both X-ray and neutron scattering; no other correction factors were included in the calculation.

Results and discussion

Mass density

All simulations described were carried out at 298 K. The mass density of the systems was obtained from the converged volume during the constant NPT run. The density of pure TBP converged to 0.9750 g/cc as against the experimental value[39] of 0.9708 g/cc, whereas for *n*-octane it was 0.7043 g/cc as against the experimental value[40] of 0.7032 g/cc. Densities of the systems are provided in Table 2.

Radial distribution function

The radial distribution functions (RDFs) between atoms belonging to different molecules were calculated. The polar core of TBP consists of phosphorus, doubly-bonded oxygen (O2 type) and three singly-bonded oxygens (OS type), while the butyl tail forms the non-polar part of the molecule. Thus the pair correlation functions between phosphorus–phosphorus, phosphorus and the two different oxygen types can aid us with an understanding of the organization of these molecules. Another pair correlation function between phosphorus and the terminal carbon (of type C_d) of the butyl tail was also calculated in order to see how the butyl tails are distributed around the phosphorus atom.

Table 2. Calculated density values of TBP/*n*-octane solutions at 298 K

System (% TBP)	Density (g/cc)
100	0.975
90	0.951
75	0.914
50	0.850
25	0.781
10	0.756
0	0.704

The P–P radial distribution function (Figure 2) shows a broad peak starting at around 6 Å. A close examination reveals the existence of a shoulder at 4.5 Å whose intensity increases with TBP concentration. Near neighbour phosphorus atoms could be distributed around a phosphorus atom in two different orientations. Due to the presence of large butyl groups, it is difficult for two phosphorus atoms belonging to two different TBP molecules to approach each other from the hydrophobic side. Instead, they approach each other from the P=O direction; it is likely that intermolecular dipole–dipole interactions between the two P=O groups aid in this process. We shall discuss the orientational preferences further in the next section. The integral of the P–P $g(r)$ up to the first coordination shell provides the coordination numbers which are listed in Table 3.

A maximum of two TBP molecules can be present within the first neighbour shell of a given TBP; however, the coordination number decreases rapidly with decreasing TBP concentration in *n*-octane. This observation is consistent with analyses of X-ray and neutron scattering data[30].

The P–O2 radial distribution function is shown in Figure 3. Three main features can be observed within the first coordination shell. The closest distance between phosphorus and oxygen (O2) is determined by the first shoulder in the P–P RDF, which is present at 4.5 Å. Given that the P=O bond length is 1.48 Å, we can expect a similar shoulder in the P–O2 $g(r)$ at around 3 Å. Indeed, such a feature is present at 3.1 Å in Figure 3. Following the same line of thought, we can see the subsequent shoulder in the P–O2 RDF at around 4.5 Å, which is likely to be related to the peak present in the P–P RDF at 6 Å. These observations hint at the likely orientation of the P=O bond vectors, which we take up in detail later.

Figure 4 shows how the oxygen atoms (OS) are distributed around the phosphorus atom in two different TBP molecules. The butyl tails are free to rotate and can fold onto themselves (various conformations) as well. As mentioned earlier, they inhibit the phosphorus atoms to approach directly along their direction. However, the P=O vector can have two different orientations, perpendicular and anti-parallel. When the P=O vectors lie perpendicular to each other, the distance between phosphorus and oxygen atom (OS) can have two different values. Phosphorus–oxygen (OS) pairs have their closest distance at around 4 Å and another clear shoulder at around 5.5 Å. But, in the perpendicular orientations of P=O vectors, the double-bonded oxygen atoms (O2) come close to each other, while the single-bonded oxygens (OS) atoms containing the butyl tails remain separated by a large distance. Hence, the distance between phosphorus and oxygen (OS) atoms increases in this orientation. Thus, when P=O vectors are anti-parallel to

Table 3. P–P coordination numbers calculated at the minimum of the first peak in the corresponding P–P pair correlation function

System (% TBP)	Coordination number
100	2.05
90	1.87
75	1.59
50	1.05
25	0.52
10	0.23

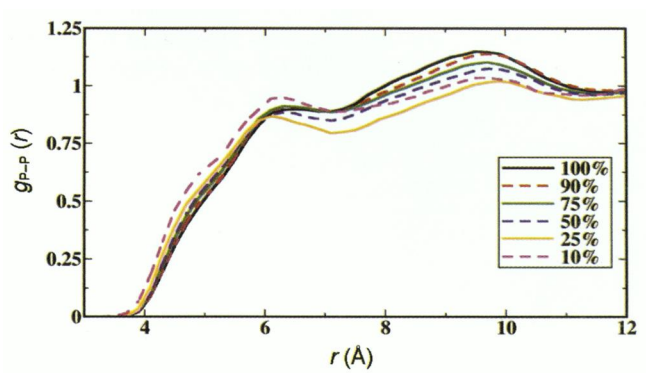

Figure 2. Intermolecular pair correlation function between pairs of atoms P–P located on two TBP molecules. Volume fraction of TBP is displayed in the legend. Features beyond 12 Å are not shown for clarity.

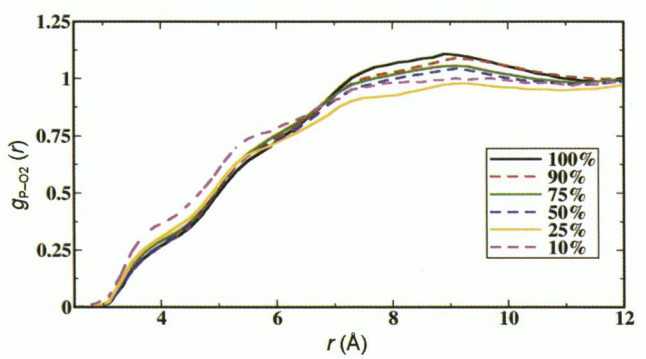

Figure 3. Intermolecular pair correlation function between pairs of atoms P–O2 on two TBP molecules.

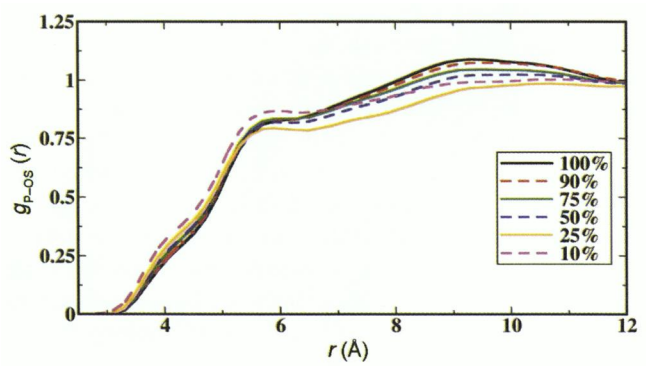

Figure 4. Intermolecular pair correlation function between pairs of atoms P–OS on two TBP molecules.

each other, a broad peak at around 9 Å distance in the P–OS radial distribution function is obtained.

The intermolecular P–C_d radial distribution function is shown in Figure 5. Compared to other radial distribution functions, it possesses sharper features. The first peak appears at 4.7 Å and the first neighbour shell ends at around 7 Å with a coordination number of two in the pure TBP system. The coordination number decreases with decrease in the volume fraction of TBP.

The summary of these observations is that two TBP molecules self-associate and the oligomer size is not larger than a dimer either in pure liquid TBP or in TBP–*n*–octane solutions.

Although the association between TBP molecules is weak (as indicated by the rather small value of two for the P–P coordination number in pure liquid TBP), TBP–TBP association is present even upon dilution by *n*-octane. In Table 3, we observed the reduction in P–P contacts with decrease in the concentration of TBP, as expected. Is the decrease commensurate to that in the mole fraction of TBP? In Figure 6, we plot the P–P coordination number against the mole fraction of TBP in the TBP/*n*-octane solutions. The coordination number is normalized by its value in pure liquid TBP. It increases monotonically, as expected. The ratio of this quantity to the mole fraction can be expected to be unity and independent of mole fraction, if TBP molecules were homogenously distributed in the solution. The actual behaviour of this ratio shown in Figure 6 suggests that at small fractions of TBP, there is a clear aggregation of TBP molecules in TBP/*n*-octane solutions.

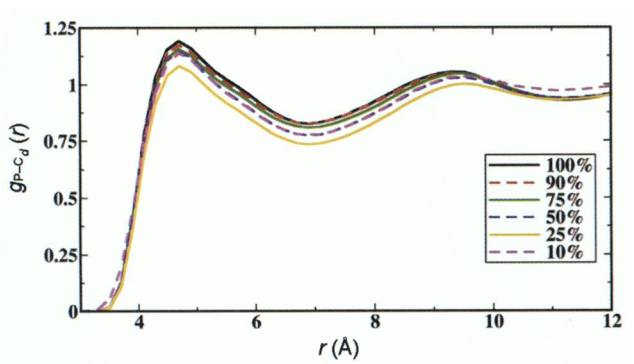

Figure 5. Intermolecular pair correlation function between pairs of atoms P–C_d on two TBP molecules. C_d refers to the terminal carbon atom of butyl tail.

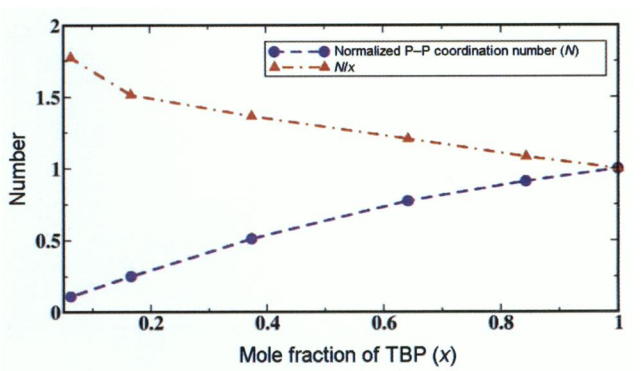

Figure 6. Normalized first coordination number between P and P in TBP/*n*-octane solutions.

Spatial distribution functions

The density distribution of atoms in three-dimensional space can be obtained from the spatial distribution functions (SDFs). We have calculated the SDF of phosphorus atoms around the centre of TBP and the same is shown in Figure 7 at an isosurface value of 0.0031 $Å^{-3}$, which is

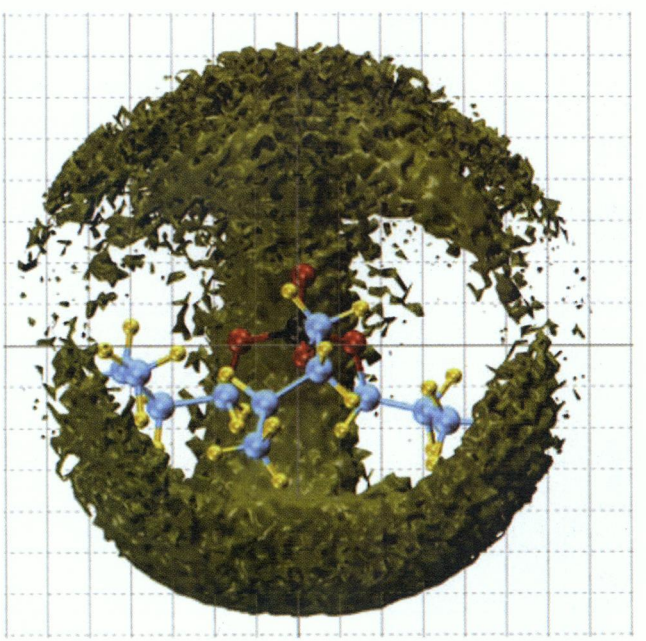

Figure 7. Spatial distribution function of phosphorus atoms around the centre of TBP in pure liquid TBP. Colours: Phosphorus – black, oxygen – red, carbon – cyan, hydrogen – orange. Grid size is 1 Å.

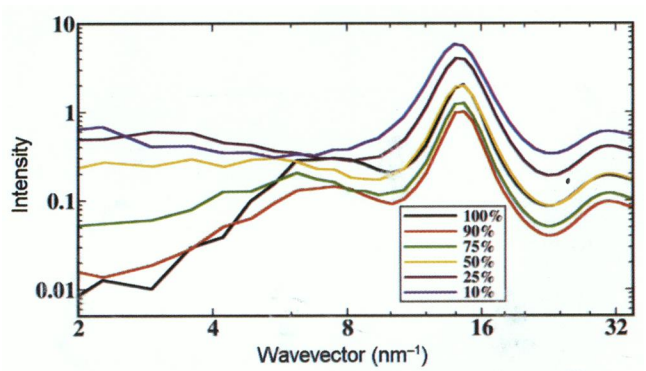

Figure 8 Total X-ray scattering intensity calculated from simulation for TBP/*n*-octane solutions.

larger than the mean number density of TBP in pure liquid TBP (0.0022 Å^{-3}). Various features observed in the radial distribution functions can be understood from the SDF. The shoulder at around 4.5 Å in the P–P $g(r)$ is due to those TBP molecules that approach each other along the P=O direction. As the large, flexible butyl tails inhibit the close approach of two TBP molecules, phosphorus atoms were found to be separated by a larger distance on the hydrophobic side.

Small angle scattering

Small angle neutron (or X-ray) scattering is a useful tool to study aggregation phenomena[49]. Figure 8 presents the total X-ray scattering intensity calculated from simulations at various compositions, while Figure 9 exhibits the same for neutron scattering. The results compare well against recent scattering experiments[30] and reproduce subtle features observed as a function of concentration of TBP. At TBP fractions of 10% and 20%, no peak can be found at $q = 6.5$ nm^{-1}, consistent with the experimental data[30]. However, a feature appears at this wave vector for concentrations beyond 50% volume fraction of TBP and whose intensity increases with TBP fraction. The position of the main peak at 6.6 nm^{-1} shifts marginally to larger wave vector values with increasing TBP concentration. It corresponds to a correlation length of 0.95 nm. The origin of this peak can be understood through an examination of the weighted partial structure factors.

Figure 10 shows a few significant neutron weighted partial structure factors for TBP/*n*-octane systems in the small q range. Partial structure factors which are not displayed in Figure 10 are either featureless in this wave vector region, or have relatively low intensities. The 6.6 nm^{-1} feature is predominantly contributed by the proton (rather deuterium) and OS–deuterium pairs. It points to a partial aggregation of the butyl tails of neighbouring TBP molecules. The 14 nm^{-1} feature, corresponding to a length scale of 0.45 nm, is contributed by pairs of carbon atoms in the tail. The distance correlates well with the expected intermolecular alkyl group separation in liquid *n*-alkanes. The weak assembly between TBP molecules can be driven by dipole–dipole interactions between P=O groups as well as by tail–tail van der Waals interactions. This result is consistent with experimental data which suggest the formation of TBP dimer in dry *n*-octane[30].

Two more peaks are present, at 14.5 and at 29.5 nm^{-1} in both X-ray and neutron scattering intensities at all TBP fractions. They arise from the intramolecular geometry of TBP and *n*-octane and hence are unimportant in the current study.

Orientation of TBP molecules

As discussed earlier, a small shoulder at around 4.5 Å along with a broad peak starting from 6.5 Å and running up to 11 Å was observed in the P–P $g(r)$. This observation suggests two different ways by which two TBP molecules approach each other. Following this idea, we have calculated the angle distribution between P=O vectors of two neighbouring TBP molecules, which is shown in Figure 11.

The P=O vectors of two neighbouring TBP molecules are distributed in two different orientations. A fraction of

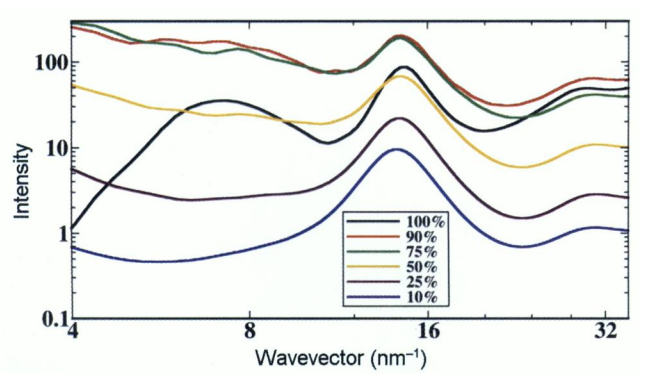

Figure 9. Total neutron scattering intensity calculated from simulation for TBP/*n*–octane–d_{18} solutions.

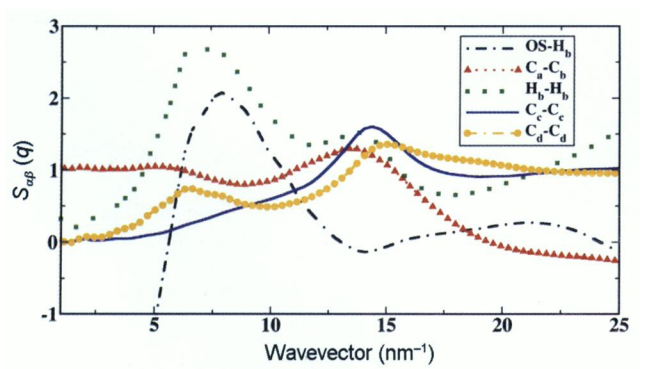

Figure 10. Neutron weighted partial structure factors calculated from simulation for pure liquid TBP.

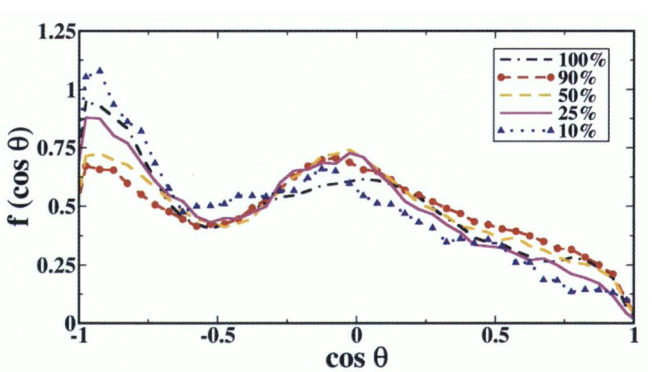

Figure 11. Distribution of angle between P=O vectors of two different TBP molecules present within 4.5 Å.

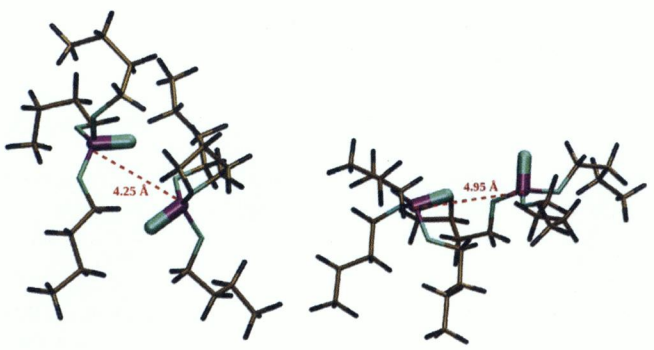

Figure 12. Two most probable orientations of P=O vectors in two different TBP molecules taken from MD simulation of liquid TBP.

neighbours is oriented with their P=O vector nearly perpendicular to each other, while a significant fraction is oriented with this angle being around 145° or more. Figure 12 shows snapshots of TBP molecules taken from the simulations at these two orientations.

Conclusion

Atomistic molecular dynamics simulations have been performed to understand the microscopic structure of TBP/*n*-octane mixtures. Wide and small angle X-ray and neutron scattering functions were calculated and compared with experimental data[30]. The computed results match the experiments closely and offer microscopic insights into the organization of TBP molecules in *n*-octane. In particular, we observe the formation of weak TBP assemblies, each containing approximately two TBP molecules oriented such that their P=O bond vectors are either nearly perpendicular or anti-parallel to each other.

The small angle X-ray and neutron profiles exhibit a peak at 6.5 nm^{-1}, whose intensity is significant at large TBP fractions. Partial structure factors demonstrate this peak to arise from tail–tail interactions at length scales of around 1.0 nm. Weak dipole–dipole interaction between the P=O groups and relatively stronger van der Waals interactions between the alkyl groups are responsible for the aggregation of TBP molecules in the pristine liquid as well as in the dry *n*-octane solutions. In particular, we observe signatures of inhomogenous distribution of TBP molecules in *n*-octane at dilute concentrations. The P–P coordination number at such concentrations is about 50% higher than what is expected from a homogenous distribution of TBP molecules in solution.

These results indicate that favourable interactions between TBP molecules in dry *n*-octane are distinctive to the results obtained for TBP reverse micelles, including water, nitric acid or heavy metal ions in their cores[24]. In the absence of water, TBP molecules do not form aggregates larger than a dimer. These structural features of TBP/*n*-octane mixtures should be useful for the future investigation of TBP reverse micelles incorporating heavy metal ions.

1. Chiarizia, R., Jensen, M. P., Borkowski, M., Ferraro, J. R., Thiyagarajan, P. and Littrell, K. C., Third phase formation revisited: the U (VI), HNO_3-TBP, dodecane system. *Solvent Extr. Ion Exchange*, 2003, **21**, 1–27.
2. Chiarizia, R., Nash, K. L., Jensen, M. P., Thiyagarajan, P. and Littrell, K. C., Application of the baxter model for hard spheres with surface adhesion to SANS data for the U(VI)-NO_3, TBP-*n*-dodecane system. *Langmuir*, 2003, **19**, 9592–9599.
3. Panja, S., Mohapatra, P., Tripathi, S., Gandhi, P. and Janardan, P., A highly efficient solvent system containing {TODGA} in room temperature ionic liquids for actinide extraction. *Sep. Purif. Technol.*, 2012, **96**, 289–295.
4. Lo, C. T., Baird, M. H. I. and Hanson, C., *Handbook of Solvent Extraction*, Wiley, New York, 1983.
5. Tedder, D. W., Schultz, W. W., Navratil, Z. D. and Kertes, A. S., In *Science and Technology of Tributyl Phosphate*, CRC Press, Boca Raton, 1991, pp. 35–70.
6. Zilberman, B., Fedorov, Y., Kopyrin, A., Arkhipov, S., Blazheva, I. and Glekov, R., Extraction of U (IV) and U (VI) with 30% tributyl phosphate under conditions of formation of the second organic phase. *Radiochemistry*, 2001, **43**, 172–176.
7. Plaue, J., Gelis, A., Czerwinski, K., Thiyagarajan, P. and Chiarizia, R., Small-angle neutron scattering study of plutonium third phase formation in 30% TBP/HNO_3/alkane diluent systems. *Solvent Extr. Ion Exchange*, 2006, **24**, 283–298.
8. Chiarizia, R., Jensen, M. P., Rickert, P. G., Kolarik, Z., Borkowski, M. and Thiyagarajan, P., Extraction of zirconium nitrate by TBP in *n*-octane: influence of cation type on third phase formation according to the 'sticky spheres' model. *Langmuir*, 2004, **20**, 10798–10808.
9. Nave, S., Mandin, C., Martinet, L., Berthon, L., Testard, F., Madic, C. and Zemb, T., Supramolecular organisation of tri-*n*-butyl phosphate in organic diluent on approaching third phase transition. *Phys. Chem. Chem. Phys.*, 2004, **6**, 799–808.
10. Vasudeva Rao, P. R. and Kolarik, Z., A review of third phase formation in extraction of actinides by neutral organophosphorus extractants. *Solvent Extr. Ion Exchange*, 1996, **14**, 955–993.
11. Ellis, R. J. and Antonio, M. R., Coordination structures and supramolecular architectures in a cerium(III)-malonamide solvent extraction system. *Langmuir*, 2012, **28**, 5987–5998.
12. Verma, P. K., Pathak, P. N., Mohapatra, P. K., Aswal, V. K., Sadhu, B. and Sundararajan, M., An insight into third-phase formation during the extraction of thorium nitrate: evidence for aggregate formation from small angle neutron scattering and validation by computational studies. *J. Phys. Chem. B*, 2013, **117**(33), 9821–9828.
13. Burger, L. L., Schulz, W. W. and Navratil, J. D., In *Science and Technology of Tributyl Phosphate*, CRC Press, Boca Raton, 1984, p. 25.
14. Petkovic, D. M., Kezele, B. A. and Rajic, D. R., Dipole moments of some neutral organic phosphates. *J. Phys. Chem.*, 1973, **77**, 922–924.
15. Petkovic, D. M. and Maksimovic, Z. B., On association of trialkyl phosphates. *J. Inorg. Nucl. Chem.*, 1976, **38**, 297.
16. Tsimering, L. and Kertes, A., Excess enthalpies of tri-*n*-butylphosphate + hydrocarbons. *J. Chem. Thermodyn.*, 1974, **6**, 411–415.
17. Tsimering, L. and Kertes, A. S., Enthalpies of mixing of tributylphosphate with hydrogenbonding solvents. *J. Chem. Eng. Data*, 1977, **22**, 163–165.
18. Poczynailo, A., Danesi, P. and Scibona, G., Solvation of uranyl nitrate by {TBP} in *n*-hexane by vapour pressure lowering measurements. *J. Inorg. Nucl. Chem.*, 1973, **35**, 3249–3255.

19. Dyrssen, D. and Petkovic, D., Distribution studies of tripropyl phosphate between different organic diluents and water. *J. Inorg. Nucl. Chem.*, 1965, **27**, 1381–1393.
20. Petkovic, D. M., Some correlations of trialkyl phosphates dimerization constants. *J. Inorg. Nucl. Chem.*, 1968, **30**, 603–609.
21. Nishimura, S., Ke, C. H. and Li, N. C., Chloroform as hydrogen donor to some organophosphorus compounds and long-chain tertiary alkylamines. *J. Phys. Chem.*, 1968, **72**, 1297–1300.
22. Choi, K. and Tedder, D. W., Molecular interactions in tri-*n*-butyl phosphate diluent mixtures. *Ind. Eng. Chem. Res.*, 1996, **35**, 2048–2059.
23. Alcock, K., Grimley, S. S., Healy, T. V., Kennedy, J. and McKay, H. A. C., The extraction of nitrates by tri-*n*-butyl phosphate (TBP). Part 1. The system TBP + diluent + H_2O + HNO_3. *Trans. Faraday Soc.*, 1956, **52**, 39–47.
24. Osseo-Asare, K., Aggregation, reversed micelles, and microemulsions in liquid–liquid extraction: the tri-*n*-butyl phosphatediluent–water–electrolyte system. *Adv. Colloid Interface Sci.*, 1991, **37**, 123–173.
25. Erlinger, C., Gazeau, D., Zemb, T., Madic, C., Lefrancois, L., Hebrant, M. and Tondre, C., Effect of nitric acid extraction on phase behavior, microstructure and interactions between primary Aggregates in the system dimethyldibutyltetradecylmalonamide (DMDBTDMA)/*n*-dodecane/water: a phase analysis and small angle X-ray scattering (SAXS) characterisation study. *Solvent Extr. Ion Exchange*, 1998, **16**, 707–738.
26. Baxter, R. J., Percus–Yevick equation for hard spheres with surface adhesion. *J. Chem. Phys.*, 1968, **49**, 2770–2774.
27. Menon, S. V. G., Kelkar, V. K. and Manohar, C., Application of Baxter's model to the theory of cloud points of nonionic surfactant solutions. *Phys. Rev. A*, 1991, **43**, 1130–1133.
28. Liu, Y. C., Chen, S. H. and Huang, J. S., Relationship between the microstructure and rheology of micellar solutions formed by a triblock copolymer surfactant. *Phys. Rev. E*, 1996, **54**, 1698–1708.
29. Chiarizia, R., Jensen, M. P., Borkowski, M., Thiyagarajan, P. and Littrell, K. C., Interpretation of third phase formation in the Th(IV)–HNO_3, TBP–*n*–octane system with Baxter's 'sticky spheres' model. *Solvent Extr. Ion Exchange*, 2004, **22**, 325–351.
30. Motokawa, R., Suzuki, S., Ogawa, H., Antonio, M. R. and Yaita, T., Microscopic structures of tri-*n*-butyl phosphate/*n*-octane mixtures by X-ray and neutron scattering in a wide q range. *J. Phys. Chem. B*, 2012, **116**, 1319–1327.
31. Beudaert, P., Lamare, V., Dozol, J. F., Troxler, L. and Wipff, G., Theoretical studies on tri-*n*-butyl phosphate: MD simulations *in vacuo*, in water, in chloroform, and at a water/chloroform interface. *Sol. Extr. Ion Exchange*, 1998, **16**, 597–618.
32. Beudaert, P., Lamare, V., Dozol, J. F., Troxler, L. and Wipff, G., Molecular dynamics simulations on europium nitrate complexes with neutral organophosphorus ligands. What governs the stoichiometry and extractability of the complex? *J. Chem. Soc., Perkin Trans. 2*, 1999, **11**, 2515–2523.
33. Schurhammer, R. and Wipff, G., Effect of the TBP and water on the complexation of uranyl nitrate and the dissolution of nitric acid into supercritical CO_2. A theoretical study. *J. Phys. Chem. A*, 2005, **109**, 5208–5216.
34. Baaden, M., Burgard, M. and Wipff, G., TBP at the water–oil interface: the effect of TBP concentration and water acidity investigated by molecular dynamics simulations. *J. Phys. Chem. B*, 2001, **105**, 11131–11141.
35. Schurhammer, R. and Wipff, G., Liquid–liquid extraction of pertechnetic acid (Tc VII) by tri-*n*-butyl phosphate: where is the proton? A molecular dynamics investigation. *J. Phys. Chem. B*, 2011, **115**, 2338–2348.
36. Ye, X., Cui, S., de Almeida, V. and Khomami, B., Interfacial complex formation in uranyl extraction by tributyl phosphate in dodecane diluent: a molecular dynamics study. *J. Phys. Chem. B*, 2009, **113**, 9852–9862.
37. Ye, X., Smith, R. B., Cui, S., de Almeida, V. and Khomami, B., Influence of nitric acid on uranyl nitrate association in aqueous solutions: a molecular dynamics simulation study. *Solvent Extr. Ion Exchange*, 2010, **28**, 1–18.
38. Ye, X., Cui, S., de Almeida, V., Hay, B. P. and Khomami, B., Uranyl nitrate complex extraction into TBP/dodecane organic solutions: a molecular dynamics study. *Phys. Chem. Chem. Phys.*, 2010, **12**, 15406–15409.
39. Tian, Q. and Liu, H., Densities and viscosities of binary mixtures of tributyl phosphate with hexane and dodecane from (298.15 to 328.15) K. *J. Chem. Eng. Data*, 2007, **52**, 892–897.
40. Ramos-Estrada, M., Iglesias-Silva, G. A., Hall, K. R. and Castillo-Borja, F., Experimental liquid densities of *n*-pentane, *n*-octane, and *n*-nonane and their binary mixtures from (273.15 to 363.15) K at 0.1 MPa. *J. Chem. Eng. Data*, 2011, **56**, 4461–4465.
41. Cui, S., de Almeida, V. F., Hay, B. P., Ye, X. and Khomami, B., Molecular dynamics simulation of tri-*n*-butyl-phosphate liquid: a force field comparative study. *J. Phys. Chem. B*, 2012, **116**, 305–313.
42. Martin, M. G. and Siepmann, J. I., Transferable potentials for phase equilibria. 1. united-atom description of *n*-alkanes. *J. Phys. Chem. B*, 1998, **102**, 2569–2577.
43. Martinez, L., Andrade, R., Birgin, E. G. and Martinez, J. M., PACKMOL: a package for building initial configurations for molecular dynamics simulations. *J. Comput. Chem.*, 2009, **30**, 2157–2164.
44. Plimpton, S., Fast parallel algorithms for short-range molecular dynamics. *J. Comput. Phys.*, 1995, **117**, 1–19.
45. Humphrey, W., Dalke, A. and Schulten, K., VMD: Visual molecular dynamics. *J. Mol. Graphics*, 1996, **14**, 33–38.
46. Bhargava, B. L., Devane, R., Klein, M. L. and Balasubramanian, S., Nanoscale organization in room temperature ionic liquids: a coarse grained molecular dynamics simulation study. *Soft Matter*, 2007, **3**, 1395–1400.
47. Chantler, C. T., Detailed tabulation of atomic form factors, photoelectric absorption and scattering cross section, and mass attenuation coefficients in the vicinity of absorption edges in the soft X-ray (Z = 30–36, Z = 60–89, E = 0.1 keV–10 keV), addressing convergence issues of earlier work. *J. Phys. Chem. Ref. Data*, 2000, **29**, 597–1056.
48. Chantler, C. T., Theoretical form factor, attenuation, and scattering tabulation for Z = 1–92 from E = 1–10 eV to E = 0.4–1.0 MeV. *J. Phys. Chem. Ref. Data*, 1995, **24**, 71–643.
49. Haldar, J., Aswal, V. K., Gyal, P. S. and Bhattacharya, S., Aggregation properties of novel cationic surfactants with multiple pyridinium headgroups. Small-angle neutron scattering and conductivity studies. *J. Phys. Chem. B*, 2004, **108**, 11406–11411.